JCTC Journal of Chemical Theory and Computation

Article

pubs.acs.org/JCTC

Nonequilibrium Molecular Simulations of New Ionic Lubricants at Metallic Surfaces: Prediction of the Friction

Ana C. F. Mendonça, Agílio A. H. Pádua, and Patrice Malfreyt[†,*]

[†]Institut de Chimie de Clermont-Ferrand, UMR 6296, Université Blaise Pascal & CNRS, 63171 Aubière, France

ABSTRACT: We report nonequilibrium molecular dynamics of ionic liquids interacting with metallic surfaces. A specific set of interaction parameters for ionic liquids composed of alkylammonium cations and alkylsulfonate anions with an iron surface, which has been previously developed (*J. Chem. Theory Comput.* **2012**, *8*, 3348) is used here. We develop a procedure for a quantitative prediction of the friction coefficient at different loads and shear rates. The simulated friction coefficient agrees very well with the available experimental ones. The dependence of friction on the load, shear velocity, surface topology, and length of alkyl side chains in the ionic liquid is also investigated. The changes in the frictional forces are explained in terms of the specific arrangements and orientations of groups forming the ionic liquid at the vicinity of the surface.

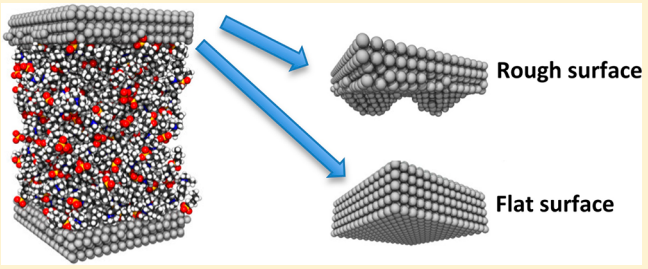

1. INTRODUCTION

The description of the molecular interactions occurring at the nanoscale between a surface and a liquid is crucial to understand the origins of friction, lubrication, wear, and adhesion.[1] Ionic liquids have been considered in the past decade as promising candidates for tribological applications.[2−5] Their remarkable properties[6] suitable for lubrication include negligible vapor pressure, nonflammability, high thermal-oxidative stability, and reasonable viscosity−temperature behavior.[7] The reason why these properties are so important for lubrication is that at the surfaces contact points the temperature will increase due to friction; therefore, the thermo-oxidative stability of the lubricant is essential to minimize its degradation during sliding. For the same reason and also for storage purposes, the nonvolatility and nonflammability are very important properties when choosing lubricant oil. The viscosity behavior of the ionic liquid is also an important property, since it determines the load-carrying capacity of the fluid and the film formation at the sliding surfaces.

Ionic liquids are complex organic salts composed of large and flexible ions typically having nonpolar side chains in their molecular structures. There are thousands of possible combinations of anions and cations, allowing the build up of task-specific compounds by adjusting key intermolecular forces. As such, melting points, viscosities, and other thermophysical properties can be fine-tuned for a specific application, by selecting different functional groups in the cation or the anion or, for example, by having different lengths in the alkyl side chains. Furthermore, due to their polar structure ionic liquids can promote the formation of an adsorbed film at the sliding surfaces, contributing to the reduction of friction and wear.[2]

Generally, ionic liquids can be used as net lubricants or additives for common (polar) lubricant oils. This last possibility has been largely explored in the past few years since the presence of ionic liquid as additives can enhance the antiwear behavior of the lubricant oil by preventing some tribochemical reactions at the surface, such as corrosion and oxidation.[8,9]

Among the possible cationic moieties, imidazolium ionic liquids are by far the most studied structures, followed by ammoniums. The works of Liu and co-workers showed the excellent tribological performance of several imidazolium based ionic liquids and their antiwear/anticorrosion properties when used as additives for poly(ethylene glycol)[10] and polyurea grease.[11] In the present study, a new group of ionic liquids based on alkylammonium cations (N_{11R4}^{+}) and alkylsulfonate anions ($C_nSO_3^{-}$) with different alkyl side chains will be used[12] (Figure 1). The length of the alkyl side chain can play an important role in the tribological performance of an ionic liquid by influencing the fluid film formation at the surface. It is reported that ions with bigger alkyl side chains can improve the friction coefficient and antiwear properties of the fluid as a consequence of the increased viscosity.[13]

The choice of the ammonium cations is linked to their potential application as lubricants or additives when associated with bistriflamide[14,15] anions. The sulfonate anions were chosen due to their low environmental impact when compared to the most commonly used fluorinated anions.[16,17]

The ordering and interactions occurring at the solid−liquid interface can have great influence in the performance of a lubricant. The nanoscale organization of ionic liquids at metallic surfaces was already described experimentally. Spectroscopic studies with imidazolium based ionic liquids in a platinum surface evidenced the formation of a very strong first solvation layer of approximately 5 Å, which corresponds to the cation−anion pair thickness.[18] Furthermore, AFM measurements in a gold surface show that the organization at the interface is only extended for

Received: October 11, 2012
Published: January 18, 2013

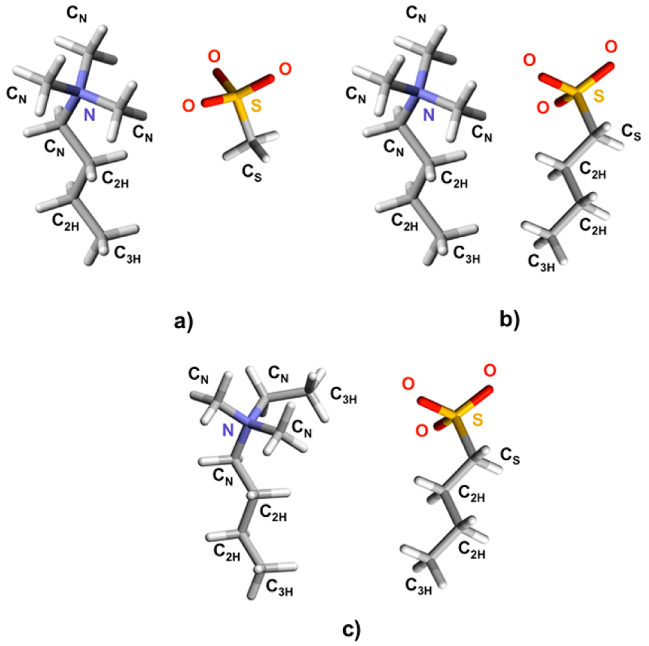

Figure 1. Molecular structures of the simulated ionic liquids, which have different alkyl side chains in the cation or the anion: (a) 1-butyl-1,1,1-trimethylammonium metanesulfonate $[N_{1114}][C_1SO_3]$; (b) 1-butyl-1,1,1-trimethylammonium butanesulfonate $[N_{1114}][C_4SO_3]$; and (c) 1-butyl-1-ethyl-1,1-dimethylammonium butanesulfonate $[N_{1124}][C_4SO_3]$.

three of four layers,[19] since the innermost layers of ions in the ionic liquid will tend to screen the electric field coming from the metallic structure. For this, the surface charge on the metal will also reflect the number of ordered layers present at the interface.

Several authors also confirmed such behavior by molecular dynamics simulation.[20−22] In particular, the adsorption of sulfonate anions in a surface of iron and the molecular ordering of the cation and anion head-groups was analyzed in a previous study.[23]

Experimental studies with molecularly thin films of ionic liquid between mica surfaces as a function of the surface separation reveal very low friction coefficients for surface separations that correspond to favorable ion packing. Furthermore, due to the charge in the ions there is the formation of a robust film of fluid between the surfaces that lasts up to high values of load, more than similar films of uncharged molecules.[24] This strong film of liquid can prevent serious breakdown of the material's asperities if the surface is rough. In fact, in the asperity−asperity contact points, the resulting high temperatures can induce chemical reactions between the fluid and the surface, promoting the formation of a boundary film, which can help to prevent severe wear of the sliding pairs.[2]

According to the laws of Amontons and Coulomb,[25,26] the friction force is directly proportional to the applied load (Amontons' first Law) and independent of the contact area (Amontons' second Law) and sliding velocity (Coulomb's first Law). Advances in nanotechnology with the build-up of "tip-based" machinery together with consistent molecular simulations of many-body dynamics demonstrated that the classical friction laws are only valid approximately. Friction does depend on the sliding velocity; these laws are not valid over large ranges of loads,[27] and they do not take into account the presence of adhering surfaces. Despite these, Amontons' and Coulomb's laws are remarkably well obeyed for a wide range of materials (rough or smooth) such as wood, ceramics, and metals, as long as they are nonadhesive. Therefore, it is important to understand the mechanisms of adhesion when dealing with metallic surfaces and organic lubricants, the object of this study. As an example of one of the consequences of adhesion is that friction in a fresh contact will be different from the one in a contact that already has undergone some sliding.

Molecular simulations have been already used to study the frictional properties of lubricating systems.[28−32] However, investigations on the structure, interactions, and molecular ordering at the interface, that can help to gain insights about lubricant performance, are much less widespread. This is probably due to the difficulty to describe liquid-surface interactions. Moreover, if a metallic surface is present, which is in the case of this work, the complexity increases. An intermolecular potential that describes liquid−metal interactions has to take into account not only van de Waals forces but also Coulombic forces arising from polarization of the metal. Metal surfaces are conductive and highly polarizable; therefore, when in contact with charged entities like ionic liquids, many-body interactions will occur that cannot be neglected. Therefore, the correct representation of the metal charge fluctuations is dependent on the nearby liquid structure, and the representation of the liquid structure itself is also dependent on the metal polarizability.[21,33] A Lennard-Jones potential is sometimes not sufficient to describe such complex interactions and other potential functions are required. For that, a model was previously build specifically for the ionic liquids in this work interacting with an iron surface, which also takes into account metal polarization. This potential model will be used in the present work.[23]

The study of the rheological properties of a lubricating system through molecular simulations is normally associated to nonequilibrium molecular dynamics, characterized by the imposition of a certain shear velocity to one of the surfaces. Commonly, load is also applied in the normal direction. When the system is in local mechanical and thermal equilibrium, properties such as the friction coefficient, friction force, and normal force can be extracted, as well as microscopic structure, energetics, and dynamic quantities. Several studies document the use of nonequilibrium simulations for the calculation of friction.[28−31,34−36] Despite this, studies involving ionic liquids are quite scarce.[37]

In the present study, we investigate by nonequilibrium molecular dynamics, the molecular ordering, and rheological properties of ionic liquids at a metallic surface under shear. A method based on a definition of pressure measured locally will be used to analyze the dependence of the friction on load, shear rate, and surface topology. This method has already been applied to measure the friction coefficient of grafted polymer chains with coarse grain models[38] and with dissipative particle dynamics approach.[39−43] Nevertheless, such methods have not been widely applied with atomistic models due to the difficulty of calculating the pressure tensor with electrostatics in a two-dimensional simulation cell. Our purpose is to mimic the experimental conditions by modeling the interactions between the ionic liquid and shearing surfaces. We aim to demonstrate that the methodology used here allows an accurate calculation of the tangential and normal elements of the pressure tensor, which are key-elements in the prediction of the kinetic friction coefficient.

2. COMPUTATIONAL METHODOLOGY

2.1. Description of the System. Each simulated system was composed of 200 ion pairs of ionic liquid confined between

dx.doi.org/10.1021/ct3008827 | J. Chem. Theory Comput. 2013, 9, 1600−1610

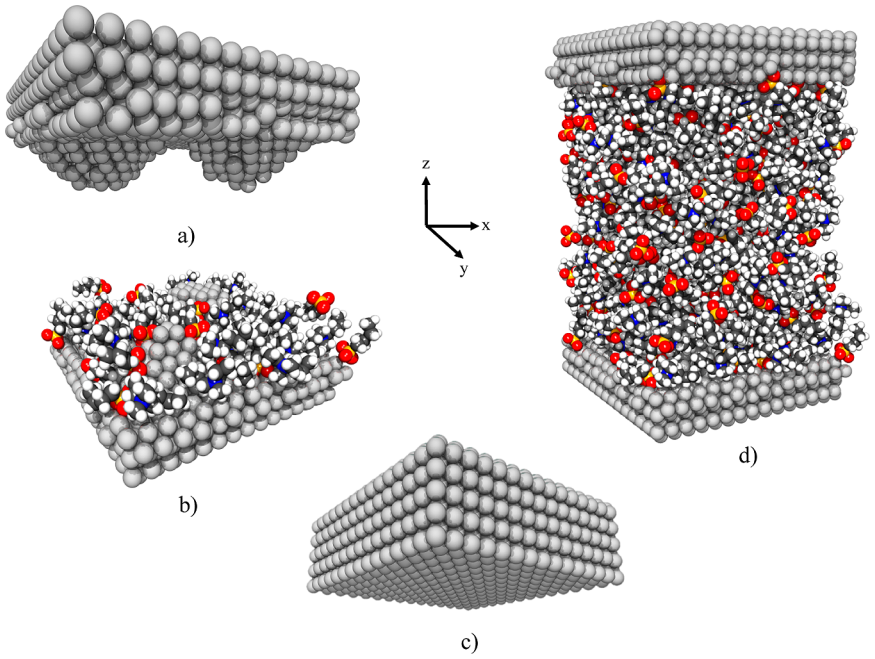

Figure 2. Snapshots of the simulated system: (a) topology of the rough surface, with two different asperities; (b) representation of the innermost (mobile) region of the metal surface that will be in direct contact with the liquid and that will be thermostatted; (c) representation of the flat surface; (d) snapshot of the equilibrated cell, a slab 200 pairs of ionic liquid confined between two surfaces of bcc iron.

surfaces of iron. Three ionic liquids containing different alkyl chains in the cation or the anion were studied: 1-butyl-1,1,1-trimethylammonium metanesulfonate ($[N_{1114}][C_1SO_3]$), 1-butyl-1,1,1-trimethylammonium butanesulfonate ($[N_{1114}][C_4SO_3]$), and 1-butyl-1-ethyl-1,1-dimethylammonium butanesulfonate ($[N_{1124}][C_4SO_3]$) (Figure 1).

The simulation box is a rectangular parallelepiped of dimensions $L_xL_yL_z$ ($L_x = L_y = 43$ Å, L_z variable) with periodic boundary conditions applied in the three dimensions.

Two types of surfaces were studied: a rough and a flat surface. Each rough surface was composed of 1572 Fe atoms and each flat surface of 1200 Fe atoms. Both surfaces were in a (001) plan of a body-centered cubic crystal (bcc) lattice. The rough surface contains two asperities having the geometry of truncated cones with radius 12 Å and 10 Å, and a height of 8 Å. The topology of the surfaces can be seen in Figure 2. Each metallic structure was build to have two distinct regions: an outermost region composed of four monolayers of iron atoms and an innermost region, which also included the asperities in the case of the rough surface. The outermost region, which will not be in direct contact with the liquid, was kept rigid during the simulations meaning that it is able to move as a solid block. To this region, velocity and load will be applied. The innermost region, which is in direct contact with the liquid, is completely mobile.

2.2. Force Field Description. In systems composed by a solid and a liquid that are three types of interactions to take into account: liquid−liquid (IL−IL), solid−solid (M−M), and solid−liquid (M−L). The potential function of the system (U) will have contributions from all of these interactions:

$$U = U_{IL-IL} + U_{M-M} + U_{M-L} \quad (1)$$

The functional form of the force field for the ionic liquid (U_{IL-IL}), describing liquid−liquid interactions, is decomposed into four kinds of potential energy associated with different modes: stretching of covalent bonds (U_{bonds}), bending of valence angles (U_{angles}), torsion around dihedral angles ($U_{torsion}$) and nonbonded interactions, with contributions from Lennard-Jones (U_{LJ}) and Coulomb (U_{Elec}) forces within the liquid (eq 2).

$$\begin{aligned} U_{IL-IL} &= U_{bonds} + U_{angles} + U_{torsions} + U_{LJ} + U_{Elec} \\ &= \sum_{ij}^{bonds} \frac{K_{r,ij}}{2}(r_{ij} - r_{0,ij})^2 + \sum_{ijk} \frac{K_{\theta,ijk}}{2}(\theta_{ijk} - \theta_{0,ijk})^2 \\ &+ \sum_{ijkl}^{torsions} \sum_{n=1}^{4} \frac{k_{n,ijkl}}{2}[1 + (-1)^{n+1}\cos(n\varphi_{ijkl})] \\ &+ \sum_{i=1}^{N-1} \sum_{j>i}^{N} \left\{ 4\varepsilon_{ij}\left[\left(\frac{\sigma_{ij}}{r_{ij}}\right)^{12} - \left(\frac{\sigma_{ij}}{r_{ij}}\right)^{6}\right] + \frac{1}{4\pi\varepsilon_0}\frac{q_iq_j}{r_{ij}} \right\} \end{aligned} \quad (2)$$

The first three terms of eq 2 are related to the interactions occurring within the same molecule, and the fourth term corresponds both to intermolecular forces between atoms of different molecules and also to nonbonded, intramolecular forces, that is, interactions occurring between different atoms of the same molecule that are distant by more than three bonds. The ion−ion interactions were represented by an all-atom force field based on the OPLS-AA model,[44,45] that was specifically parametrized for the ionic liquids present in this work.[46,47]

Metal−metal interactions (U_{Metal}) are described by a Finnis−Sinclair potential,[48,49] a nonadditive form that allows to describe the bonding of metal atoms in terms of the local density. To account for the induced charges on the metallic conductor surface by the ions, the metal atoms were made polarizable by employing a Drude-rod model developed by Iori and Corni,[50] which consists in the addition of an embedded dipole into each metal atom. The dipole is free to rotate in response to the local electric field and will interact electrostatically with the point charges in the ions of the liquid. Two opposite charges (q) are separated by a distance (l_0) and have the same mass (m). The parameters used herein are $l_0 = 0.7$ Å, $m = 0.5$ au, $q = 0.3$ e.

dx.doi.org/10.1021/ct3008827 | J. Chem. Theory Comput. 2013, 9, 1600−1610

The interactions that are most complex to describe in this type of systems are those corresponding to the solid−liquid interactions. A model derived from first principles was build specifically for the ionic liquids in this work interacting with a surface of iron. In this potential, the ionic system composed by alkylammonium cations and alkylsulfonate anions was split into three fragments: butane (C_4H_{10}), tetramethylammonium (N_{1111}^+), and methylsulfonate ($CH_3SO_3^-$), studied at different distances and orientations from a bcc cluster of 21 iron atoms. The interaction energies obtained from ab initio calculations were then fitted with a classical site−site potential function of the type *nm*[51] and added with a Coulombic term to account for the metal polarization, by the ions. Equation 3 describes this form of potential.

$$U_{M-L} = \sum_{i=1}\sum_{j=1}\frac{E_0}{(n-m)}\left[m\left(\frac{r_0}{r_{ij}}\right)^n - n\left(\frac{r_0}{r_{ij}}\right)^m\right] + \frac{q_i q_j}{r_{ij}} \quad (3)$$

The full description of the model and the parameters of interaction E_0, n, m, and r_0 can be found elsewhere.[23] It is important to point that this is an atom−atom model, and therefore, it is independent of the surface topology and thus can be used to represent either flat or rough surfaces.

2.3. Nonequilibrium Molecular Dynamics. The LAMMPS molecular dynamics package[52] was used to perform all simulations. The initial configuration was a low-density lattice containing both the ionic liquid and the surfaces that was equilibrated in the NVE ensemble from 0 K to 500 K, by small temperature increments. All C−H bonds of the ionic liquid and the Fe-q bonds of the Drude dipoles on the metal were constrained using the SHAKE algorithm.

To achieve the correct density of the bulk (~1 g·cm^{-3} for these ionic liquids), the surfaces were brought together by applying a constant velocity to the upper surface, in the $-z$ direction. When this condition was achieved, the compression was stopped and the system was further equilibrated for 1 ns with a time step of 1 fs, at constant *NVT* regulated by a Langevin thermostat. A snapshot of the equilibrated cell can be seen in Figure 2d.

A nonequilibrium simulation was then performed over 1.5 ns with a time step of 1 fs, by imposing a continuous shear velocity along the x direction to the rigid region of the upper surface, while keeping the rigid bottom surface fixed. At the same time that shear occurred, a constant force was applied in the $-z$ direction to the sheared region. A problem associated with the modeling of friction through molecular dynamics is that the kinetic energy will be converted into heat that needs to be removed in order to keep a steady state. By coupling a Langevin thermostat to the innermost regions of the surface including the asperities, the liquid lubricant was allowed to heat, and at the same time, there will be some heat dissipation through the solid.[53] All nonequilibrium simulations were performed at constant *NVT* coupled with a Langevin thermostat fixed at 500 K. We took the route of simulating the ionic liquid at 500 K rather than room temperature, since their high viscosity will lead to a slow convergence of the molecular dynamics trajectories at room temperature. Studies of the ionic liquid−vacuum interface for the prediction of the surface tension have shown that at low temperatures the strong electrostatic interactions and the slow dynamics associated to this class of fluids do not allow reliable calculations.[54] Although the force field parameters used in this study have been tested through the prediction of crystal structures and liquid densities at room temperatures, they reproduce well the temperature-dependence of the viscosity[55] and surface tension.[54]

Long-range electrostatic interactions were handled through the particle−particle particle-mesh solver[56] (P3M) with a relative accuracy of 0.0001 in the calculation of the interaction energy and a real-space cutoff of 14 Å. To apply the three-dimensional P3M method in a slab geometry using the 3D periodic boundary condition, the dimension of the simulation box was increased along the z-axis by placing 30 Å of empty space on the external sides of each surfaces.[57]

Different simulations at several values of shear rate and load were experimented, in order to study the behavior of the system as a function of such variables. Shear velocities of 0.01, 2, 4, and 15 m·s^{-1} were examined for constant loads of 1.6, 6, and 14 nN. For a constant shear velocity of 4 m·s^{-1}, different values of load were applied, 1.6, 3, 6, 10, and 14 nN, which correspond to a nominal pressure of 89, 166, 333, 555, and 776 MPa, respectively. For the nonequilibrium molecular simulations, we mimic the experimental procedure followed by Eder et al.[35]

Trajectories of all atoms were stored every 500 steps during the course of the simulation for subsequent analyses, described in the next section.

2.4. Rheological Properties. The application of a certain shear along the x-axis will create a velocity gradient in the z-direction for the particles in the fluid. It is then very important to check the thermodynamic properties along the z-axis where the heterogeneities take place. This may influence the local equilibrium properties and other dynamic properties of the liquid such as viscosity and diffusion. The local properties are averaged in each slab z_k of thickness Δz, obtained by splitting the simulation cell along the z-direction into N_{slabs}.

The average instant velocity ($v_\alpha(z_k)$) of particles in the slab z_k of the simulation box along the α direction (x, y, or z) is given by

$$v_\alpha(z_k) = \frac{\sum_{i=1}^{N} H_k(z_i)(v_i)_\alpha}{\sum_{i=1}^{N} H_k(z_i)} \quad (4)$$

where N denotes the total number of particles, $(v_i)_\alpha$ is the velocity of particle i in the direction α, and $H_k(z_i)$ is a top-hat function, defined as

$$H_k(z_i) = \begin{cases} 1, & \text{for } z_k - \frac{\Delta z}{2} < z_i < z_k + \frac{\Delta z}{2} \\ 0, & \text{otherwise} \end{cases} \quad (5)$$

The components of the pressure tensor are calculated using the Irving−Kirkwood (IK) definition[58,59] (eq 7). This definition allows a local description of the elements of the pressure tensor and leads to a correct calculation of these elements in a pseudo-two-dimensional periodic system. Using this definition, it is assumed that molecules i and j give a local contribution to the pressure tensor in a given slab, if the line joining the center of mass of i and j crosses, starts, or finishes in that slab. Each slab will have $1/N_{slabs}$ of the total contribution from the $i-j$ interaction.

$$P_{\alpha\beta}(z_k) = P_{\alpha\beta}^{kin}(z_k) + P_{\alpha\beta}^{conf}(z_k) \quad (6)$$

dx.doi.org/10.1021/ct3008827 | J. Chem. Theory Comput. 2013, 9, 1600−1610

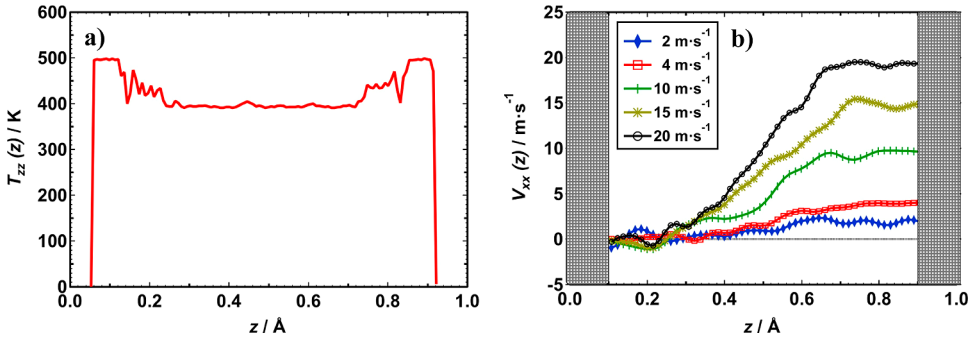

Figure 3. (a) Temperature profile of the system for a simulation at 500 K; (b) *x*-component of the velocity of all particles in the liquid, when different values of shear are applied.

$$P_{\alpha\beta}(z_k) = \langle \rho(z_k) \rangle k_B T_{\alpha\beta}(z_k) + \frac{1}{L_x L_y} \left\langle \sum_{i=1}^{N-1} \sum_{j>i}^{N} \frac{(r_{ij})_\alpha (F_{ij})_\beta}{|z_{ij}|} \theta\left(\frac{z_k - z_i}{z_{ij}}\right) \theta\left(\frac{z_j - z_k}{z_{ij}}\right) \right\rangle \quad (7)$$

Each pressure component is expressed as a sum of a kinetic term $P_{\alpha\beta}^{kin}(z_k)$ and a configurational term $P_{\alpha\beta}^{conf}(z_k)$, corresponding to the first and the second arguments of eq 6, respectively. In eq 7, $\langle \cdots \rangle$ denotes the average over all configurations of the system; $\rho(z_k)$ is the density of particles in the slab z_k; $T_{\alpha\beta}$ is the configurational temperature; r_{ij} is the distance between the center of mass of molecules i and j; $\theta(z)$ is a unit step function that is 0 for $z < 0$ and 1 elsewhere; L_xL_y is the surface area normal to the z axis; and finally $\mathbf{F}_{ij}$ represents the sum of all site−site forces acting between molecules i and j and is defined as

$$\mathbf{F}_{ij} = \sum_{a=1}^{N_i} \sum_{b=1}^{N_j} (\mathbf{f}_{iajb}) = -\sum_{a=1}^{N_i} \sum_{b=1}^{N_j} \frac{\mathbf{r}_{iajb}}{r_{iajb}} \left[\frac{dU_{ab}(r_{iajb})}{dr_{iajb}} \right] \quad (8)$$

where r_{iajb} is the distance between atom a of molecule i and atom b of molecule j and $U_{ab}(r_{iajb})$ represents the nonbonded interactions between atoms a and b and it is the sum of U_{LJ}, U_{Elec}, and U_{M-L} terms described in eq 2 and 3, respectively. A comprehensive description of the different terms can be found elsewhere.[60]

The elements of the temperature $T_{\alpha\beta}$ tensor in each slab, are defined as

$$k_B T_{\alpha\beta}(z_k) = \left\langle \frac{\sum_{i=1}^{N} H_k(z_i) m_i [(v_i)_\alpha - u_\alpha(z_k)][(v_i)_\beta - u_\beta(z_k)]}{\sum_{i=1}^{N} H_k(z_i)} \right\rangle \quad (9)$$

where m_i and $(v_i)_\alpha$ are the mass and the velocity in the α direction of particle i, respectively, and $u_\alpha(z_k)$ is the streaming velocity, defined by the average of the velocity given in eq 4.

The definition of friction based in the Amonton's first law ($F_x = \mu F_z$), is only valid for nonadhering surfaces. If these surfaces are present, a nonzero friction coefficient associated to the adhesion of lubricant particles at the surface[27,61] will exist, even when no "external" load is applied. Derjaguin[62] proposed a modified Amontons' first law (eq 10) by adding a term related to the "internal" load contribution due to the adhesion of particles at the surface (F_0):

$$F_x = F_0 + \mu F_z \quad (10)$$

where,

$$F_x = \frac{P_{xz}}{A_z}$$

and

$$F_z = \frac{P_{zz}}{A_z}$$

Therefore, we can obtain a modified Amontons first law described in terms of pressure:

$$\langle P_{xz}(z_k) \rangle = P_0 + \mu \langle P_{zz}(z_k) \rangle \quad (11)$$

where P_0 represents the adhesion-dependent contribution to the pressure and $\langle P_{xz}(z_k) \rangle$ and $\langle P_{zz}(z_k) \rangle$ are the tangential and normal components of the pressure tensor averaged over all the slabs z_k in the z-direction, over all configurations of the system (def. in eq 7). The slope of the curve between $\langle P_{xz}(z_k) \rangle$ and $\langle P_{zz}(z_k) \rangle$ will return the kinetic friction coefficient μ, for systems composed of adhering surfaces, which is the case of this work.

The term P_0 is proportional to the number of interatomic or intermolecular bonds that are broken and reformed when the adhering surfaces are rolling against each other.[63] As a consequence of this modification, the friction coefficient will be no longer independent of the load, in disagreement with Amonton's first law:

$$\mu = \frac{P_{xz} - P_0}{P_{zz}} \quad (12)$$

which gives $\mu = \infty$ when the applied pressure in the z direction is zero.

3. RESULTS AND DISCUSSION

3.1. Methodological Discussion. Since the nonequilibrium trajectories are generated in the constant−*NVT* ensemble, it is essential to check how the temperature and pressure components along the direction normal to the surface are affected by shear. Figure 3a shows the z-component of the temperature calculated from eq 9 along the z-direction, in reduced coordinates (z/L_z). Interestingly, we observe that the temperature profile is constant in the middle of the simulation cell with slight increases at the surfaces. It means that the configurations are well equilibrated with a temperature identical at each z for the bulk liquid, as expected from the thermal

dx.doi.org/10.1021/ct3008827 | J. Chem. Theory Comput. 2013, 9, 1600−1610

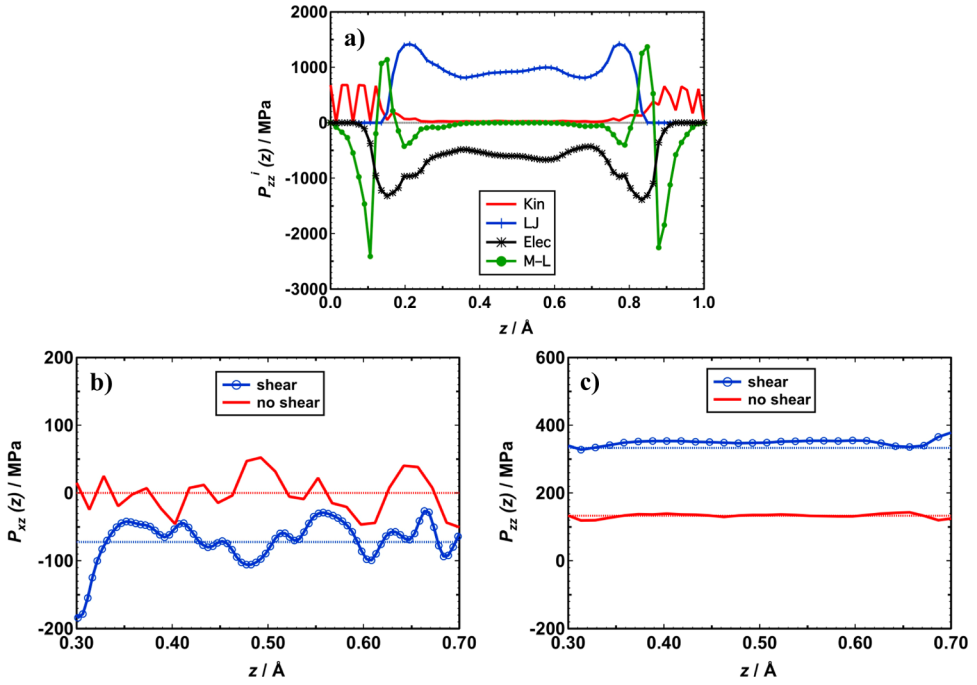

Figure 4. Different components of the pressure tensor: (a) $P_{zz}(z)$ decomposed into its contributors; (b) $P_{zz}(z)$; and (c) $P_{zz}(z)$ profiles when no shear and a constant shear velocity of 4 m·s^{-1} is applied, at 500 K.

equilibrium of the constant-*NVT* statistical ensemble. The *x*-component of the velocity of the liquid along *z*-axis (eq 4) is plotted in Figure 3b. For completeness, different sliding velocities are represented. At each sliding velocity there is a constant *z*-velocity profile close to the surface, indicating that a large fraction of ionic liquid molecules are carried by the surface as expected from the no-slip boundary condition. At a certain distance from the surfaces, the molecules exhibit a linear velocity profile, which is a characteristic of a classical Newtonian fluid. We observe that the amount of fluid in the no-slip condition decreases with the increasing sliding velocity.

We now focus on the calculation of the local elements of the pressure tensor using eq 7. Figure 4a shows the different contributions to the normal component of the pressure tensor as a function of *z*. $P_{zz}(z)$ is separated into its kinetic (Kin), Lennard-Jones (LJ), Ewald (Elec), and metal−liquid (M−L) contributors. Except for the oscillations near each surface, the different contributions show flat profiles in the bulk region that are expected for configurations at mechanical equilibrium. These oscillations come from the fact that at the surface there is a strong organization of molecules, as it can be seen by the kinetic contribution, which will be compensated by the other contributions.

The profiles are symmetric and the liquid region is wide enough to give profiles that are almost independent of *z* in the liquid region. The decomposition into the different parts shows negative and positive normal components for the electrostatic (Elec) and dispersion−repulsion (LJ) energy contributions.

Parts b and c of Figure 4 show the tangential (xz) and normal (zz) components of the pressure tensor, under no shear and at a constant shear velocity of 4 m·s^{-1}. As expected from equilibrium simulations, $P_{xz}(z)$ is zero when no shear is applied and it is negative when a sliding velocity is applied in the *x*-direction. When the system is sheared under a load of 6 nN, $P_{zz} = 352 \pm 13$ MPa. When no shear is applied, $P_{zz}(z)$ decreases to 133 ± 6 MPa. Both components of the pressure tensor are constant through the middle of the simulation box, a condition required for the local mechanical equilibrium and a good estimation of the average components.

To predict reliable kinetic friction values using molecular dynamics simulation, we must guarantee that the system is in local thermal and mechanical equilibrium. The calculation of the local pressure allowed us to evaluate the mechanical equilibrium inside the simulation cell: the normal pressure ($P_N = P_{zz}$) and the tangential pressure (P_{xz}) were constant through the simulation box for a planar interface. The temperature profiles demonstrate that the system is, in fact, in thermal equilibrium. An accurate calculation of the local elements of the pressure tensor is the key-element to predict the friction coefficient by molecular simulations. Here, we have developed methodological tools to measure the kinetic friction between ionic liquid and metal surfaces. This strategy opens the way of understanding the relationship between the structure of the ionic liquid and its lubricant properties.

3.2. Friction as a Function of Load and Shear Velocity.

In this section we present the dependence of the kinetic friction coefficient on the load and sliding velocity. The dependence on load is represented in Figure 5 for the ionic liquid $[N_{1114}]$-$[C_4SO_3]$. The average values for the P_{xz} and P_{zz} components of the pressure tensor were plotted against each together in Figure 5a. Each point represents a simulation at a given load using a constant shear velocity of 4 m·s^{-1}. Experiments at two given temperatures were performed: 350 K (red curve) and 500 K (blue curve). The slope of these curves, in agreement with eq 11, represents the kinetic friction coefficient. Values of P_0 and μ for each temperature are given in the caption of Figure 5.

The nonequilibrium molecular dynamics predict here a friction coefficient of 0.087 for 500 K and 0.149 for 350 K. Interestingly, the simulated kinetic friction coefficients are close to the ones measured experimentally for similar ionic liquid structures.[64,65] Furthermore, in most of the cases the experimental friction coefficient of systems composed of metallic

dx.doi.org/10.1021/ct3008827 | J. Chem. Theory Comput. 2013, 9, 1600−1610

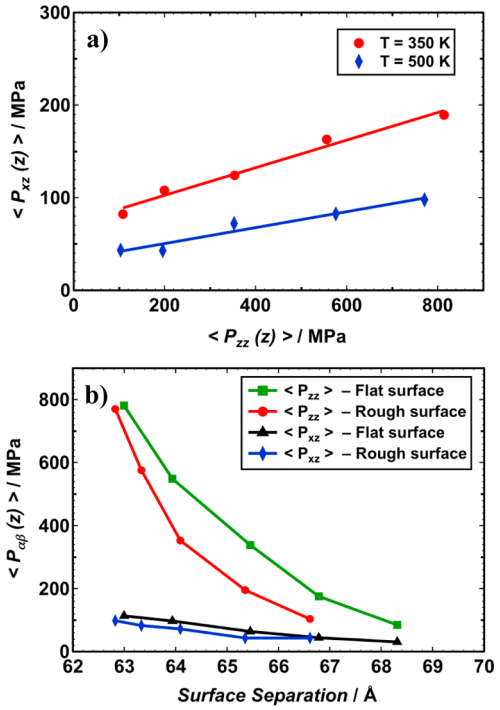

Figure 5. (a) Frictional forces P_{xz} as a function of the normal forces P_{zz}. Linear regressions give the following equations: P_{xz} = 72.7 + 0.149 P_{zz} (350 K) and P_{xz} = 31.0 + 0.087 P_{zz} (500 K). (b) P_{zz} and P_{xz} components as a function of the surface separation for two surface topologies.

surfaces in contact with ionic liquid varies between 0.05 and 0.12,[2,3,9] for a shear rate of the order of 10^{-2} m·s^{-1}. Therefore, our results predict quite well the experimental results even if the frictional force is velocity dependent, a subject of further discussion. The temperature dependence of the friction coefficient finds its origin in the temperature dependence of the tangential component (P_{xz}) of the pressure tensor whereas the normal force is very little T-dependent.

The variation of the tangential and the normal components of the pressure tensor as a function of the surface separation, which is also a measure of the applied load since higher loads imply lower surface separation, is represented in Figure 5b. It can be seen that the normal component of the pressure is more significant influenced by the surface separation. This means that high values of load are necessary to approach the two metallic surfaces. In boundary lubrication, when surface separations approach the molecular dimensions, physical adsorption of the lubricant molecules at the surface occurs (condition of no-slip) and the fluid becomes capable of supporting high loads, in agreement to what it is seen here. These findings let us to the conclusion that the ionic liquids present in this work based in alkylammonium cations and alkylsulfonate anions present a high-load carrying capacity and form a protective film of fluid at the surface, which can contribute to the reduction of friction and wear.

Until now, friction has only been discussed for a shear velocity of 4 m·s^{-1}, a value 100 times higher than the one practiced experimentally. In order to understand the behavior of the friction force with the velocity of shear, different velocities were applied to the systems under load. The tested shear velocities correspond to 0.01 (experimental value), 2, 4, and 15 m·s^{-1}. Figure 6 represents the frictional force (P_{xz}) as a function of the shear velocity for three different values of load: 1.6, 6, and 14 nN.

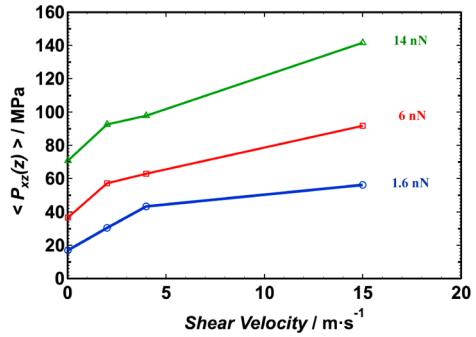

Figure 6. Dependence of P_{xz} with the shear velocity for different values of applied load.

This graph shows two features: P_{xz} increases with the applied load and with the shear velocity. In the first case, a higher applied load may signify an increase of the necessary force to maintain a continuous sliding. The same shear velocity dependence of P_{xz} was also found by other authors.[29,66] This is supposed to be associated to thermal activation at the interface, when the shear rate increases. However, within the 0.01−4 m·s^{-1} velocity range, the friction remains unchanged within the statistical fluctuations.

3.3. Friction as a Function of the Surface Topology.

Two surface topologies, a flat and a rough surface, were studied. The roughness was modeled by the introduction of two asperities with truncated cone geometry (Figure 2a). The average components of the pressure tensor, friction coefficient, and P_0 are presented in Table 1 as a function of the load. The standard deviation for the measured variables of pressure is around 10% for P_{zz} and 30% for P_{xz}, of the overall values. Simulations at different loads were performed with a constant shear velocity of 4 m·s^{-1}, for the ionic liquids $[N_{1114}][C_1SO_3]$, $[N_{1114}][C_4SO_3]$ and $[N_{1124}][C_4SO_3]$.

Interestingly, Table 1 shows that the friction coefficient of the flat surface (μ = 0.123) is higher than that of the rough surface (μ = 0.087), for the ionic liquid $[N_{1114}][C_4SO_3]$. The normal and tangential components of the pressure tensor were also plotted against the surface separation for the two types of surfaces in Figure 5b. The tangential component is slightly higher for the flat surface. In the case of the normal component of pressure, the normal force is higher for the flat surface than for the rough surface. This means that is more difficult to approach two flat surfaces than two rough surfaces, which can be associated to the high ordered adsorbed layer at the flat metallic surface. From Figure 5b, we can also conclude that the decrease of the friction coefficient with the roughness of the surface is mainly caused by the normal force and not by the weak change in the shear force.

We expect to find an explanation of this behavior by representing the local density profiles of systems at the equilibrium (no shear) and under shear, presented in Figure 7. The oxygen atoms (O) and the sulfur atom (S) are representative of the headgroup of the alkyl-sulfonate anion; the nitrogen atom (N) is representative of the positive headgroup of the alkyl-ammonium cation; and finally, the terminal carbon atoms (C_{3H}) represent the position of the longer alkyl chains in either anions or cations (Figure 1). In the graph corresponding to the flat surface at the equilibrium (Figure 7a), two layers of anion head-groups are observed, clearly marked by the peaks of S and O atoms. Logically, O atoms approach closer to the surface. Only one structured layer of cation head-groups is perceived through the strong peak of N atoms, at distances from the surface that are slightly larger than that of S atoms from the anion. Two peaks

dx.doi.org/10.1021/ct3008827 | J. Chem. Theory Comput. 2013, 9, 1600−1610

Table 1. $P_{zz}(z)$ and $P_{xz}(z)$ Components of Pressure (Eq 7), Average Friction Coefficient (μ) and Internal Pressure (P_0) Calculated Using Eq 11[a]

surface topology	imposed load (nN)	$\langle P_{zz}(z)\rangle$ (MPa)	$\langle P_{xz}(z)\rangle$ (MPa)	P_0 (MPa)	$\langle\mu\rangle$
		$[N_{1114}][C_4SO_3]$			
flat surface	1.6	85	30		
	3	176	44		
	6	338	64	22	0.123
	10	549	97		
	14	781	113		
		$[N_{1114}][C_4SO_3]$			
rough surface	1.6	103	43		
	3	196	43		
	6	352	63	31	0.087
	10	576	82		
	14	770	98		
		$[N_{1114}][C_1SO_3]$			
	1.6	57	25		
	3	141	35		
	6	348	73	22	0.112
	10	515	77		
	14	723	101		
		$[N_{1124}][C_4SO_3]$			
	1.6	107	42		
	3	199	58		
	6	277	50	26	0.132
	10	581	106		
	14	800	131		

[a]Results concern systems composed of: flat iron surface in contact with the ionic liquid $[N_{1114}][C_4SO_3]$ and rough iron surface in contact with the ionic liquids $[N_{1114}][C_1SO_3]$, $[N_{1114}][C_4SO_3]$ and $[N_{1124}][C_4SO_3]$.

corresponding to the terminal C atoms of the alkyl side chains in the cation or the anion are also present and appear further away from the surface than the charged head-groups. The second peak of the C atoms at 49 Å is slightly higher than the one at 52 Å, indicating an ordering of the alkyl tails pointing away from the metal surface. This is characteristic of the segregation between the alkyl chains, which aggregate to form nonpolar regions.[67] In general, the interfacial layer of this ionic liquid is approximately 10 Å thick, and it is composed of anion and cation head-groups separated by 2 Å and a second, less-ordered layer of anions.

The corresponding system under shear is represented in Figure 7c. Here, the intensity of the O and N atoms increases, as a result of the applied load in the normal direction. The position of the peaks is maintained. From the velocity profiles, we observe that the region of the constant velocity along z-axis corresponds to that of the two layers of anion head groups indicating a strong interaction with the surface under shear.

Concerning the system with rough surfaces (Figure 7b), the main difference in terms of local density profile from the system discussed above is a reduction in the height of the peaks and in the molecular ordering at the interface. Furthermore, when shear is applied (Figure 7d), a decrease in the intensity of all peaks corresponding to the cation−anion layer closer to the surface is observed. These findings may be associated with the lower friction for this last system when compared to the one with the flat surface. The ordering of the adsorbed film of fluid at the interface in the case of the flat surface seems to be more significant than for the rough surface system, which can have some influence on friction.

The orientation of the alkyl side chains in the anion or the cation with respect to the metallic surface was analyzed with the aid of a Legendre polynomial function:

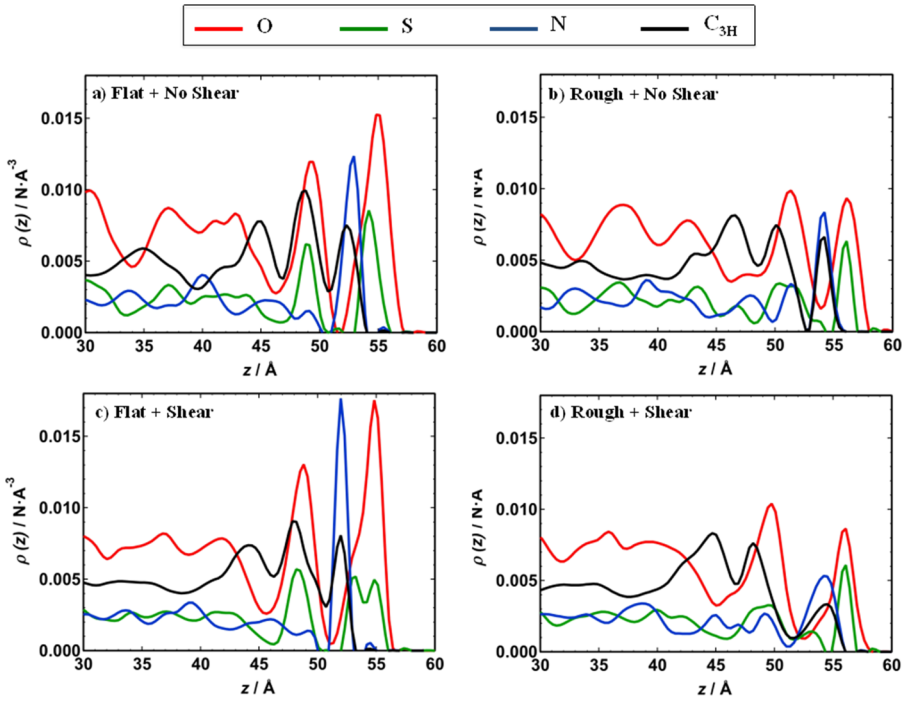

Figure 7. Atomic density profiles of O (red), S (green), N (blue), and C_3H (black) atoms, for the following systems: (a) flat surface under zero shear; (b) rough surface under zero shear; (c) flat surface under a shear velocity of 4 m·s^{-1}; (d) rough surface under a shear velocity of 4 m·s^{-1}. The systems under shear were also submitted to a constant load of 6 nN. Both surfaces were in contact with the ionic liquid $[N_{1114}][C_4SO_3]$.

dx.doi.org/10.1021/ct3008827 | J. Chem. Theory Comput. 2013, 9, 1600−1610

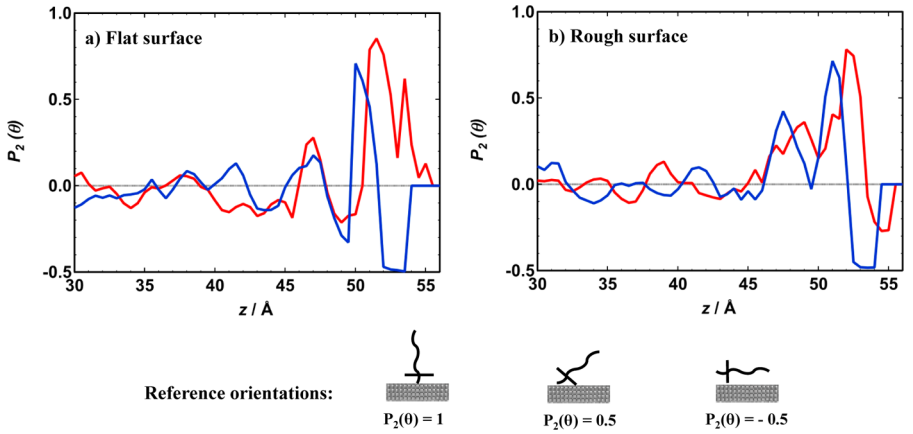

Figure 8. Orientational ordering parameter, $P_2(\theta)$, for the ionic liquid $[N_{1114}][C_4SO_3]$ in contact with (a) flat surface and (b) rough surface. The red curves represent the orientation of the anions, and the blue curves represent those of the cations. The reference orientation of the alkyl side chains is illustrated in the figure.

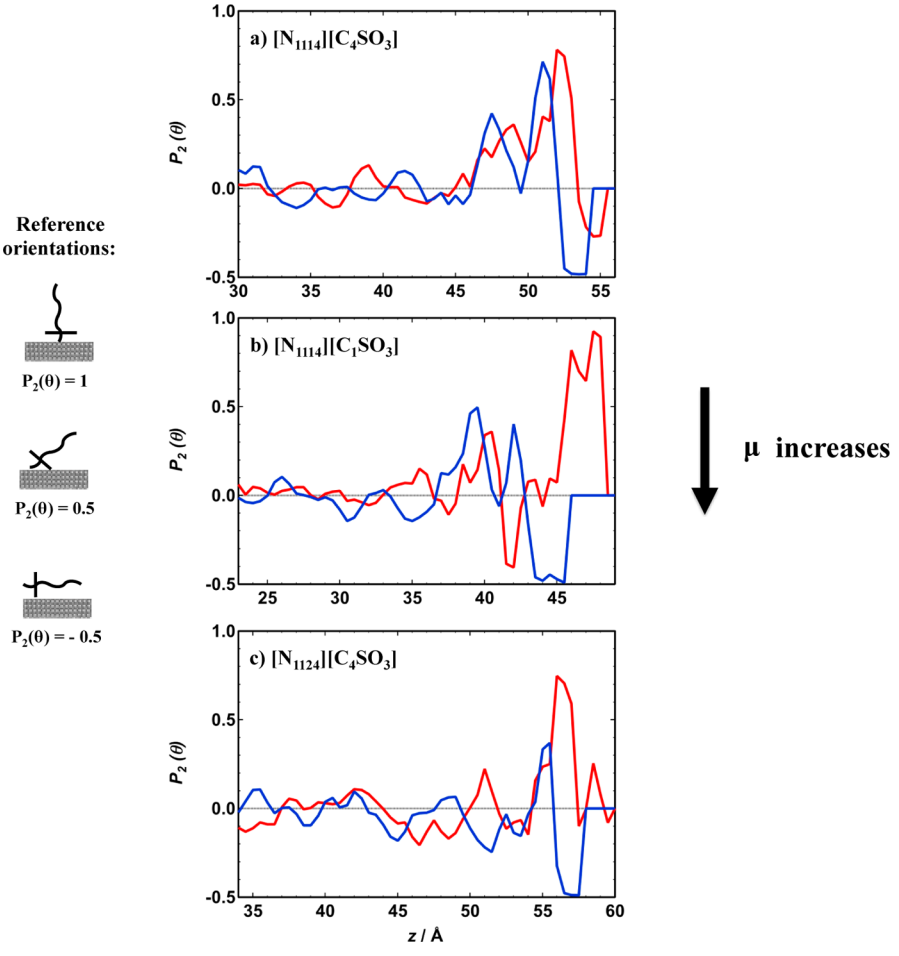

Figure 9. Orientational ordering parameter, $P_2(\theta)$, for the ionic liquids (a) $[N_{1114}][C_4SO_3]$, (b) $[N_{1114}][C_1SO_3]$, and (c) $[N_{1124}][C_4SO_3]$ in contact with a rough surface. The red curves represent the orientation of the anions and the blue curves those of the cations. The reference orientation of the alkyl side chains and the trend of the friction coefficient are represented in the figure.

$$\langle P_2(\theta)\rangle = \left\langle \frac{1}{2}(3\cos^2(\theta) - 1) \right\rangle \tag{13}$$

where θ is the angle between the surface normal and a vector chosen in the ion. In the present ionic liquids, both cations and anions are composed of an essentially spherical headgroup (trimethylammonium or sulfonate) and an alkyl side chain; therefore, the vector representing the orientation of the ions was defined between a central atom of the cation or anion headgroup (i.e., N or S) and the terminal atom of the respective alkyl side chain, that is, C_S for $[N_{1114}][C_1SO_3]$ or C_{3H} for $[N_{1114}][C_4SO_3]$ and $[N_{1124}][C_4SO_3]$). $P_2(\theta)$ varies from 1 to −0.5. A value of 1 indicates that the vector on the ion is parallel to the surface normal and therefore the alkyl side chains are perpendicular to

dx.doi.org/10.1021/ct3008827 | J. Chem. Theory Comput. 2013, 9, 1600−1610

the metal surface. A value of −0.5 means that the vectors are perpendicular and the preferred orientation of the side chains is parallel to the metal surface. Figure 8 presents the orientations of the alkyl side chains in the cation (blue curves) and the anion (red curves) for the ionic liquid $[N_{1114}][C_4SO_3]$ in contact with flat and rough surfaces.

For the flat surface the first peaks of the anion correspond to an orientation of the alkyl tails that is essentially perpendicular to the metal surface, after which the orientation becomes random and $P_2(\theta)$ decays to zero as expected for bulk configurations. In the case of the cation, the alkyl side chains closer to the surface have a parallel orientation for ∼2 Å, after what it becomes perpendicular. This means that the alkyl chains of the first layer of cations and anions have different orientations toward the surface. This behavior differs in the rough surface. Actually, the cation and the anion side chains are in phase with each other and adopt the same orientation at the interface; that is, they are parallel for the layers closer to the surface and perpendicular afterward. The fact that they have the same orientation can promote the segregation of the alkyl tails and create nonpolar domains at the interface, which may promote sliding. Experimentally, it is known that the increase of the number of carbons in the alkyl tails reduces the friction coefficient.

3.4. Friction as a Function of the Ionic Liquid Structure. Friction was measured for three ionic liquids interacting with a rough iron surface (see Table 1). It can be observed that the friction coefficient for the ionic liquid $[N_{1114}][C_4SO_3]$ is the lowest ($\mu = 0.087$), followed by $[N_{1114}][C_1SO_3]$ ($\mu = 0.112$) and $[N_{1124}][C_4SO_3]$ ($\mu = 0.132$). When looking to the structures of $[N_{1114}][C_4SO_3]$ and $[N_{1114}][C_1SO_3]$, one expects that the friction coefficient increases with shorter alkyl side chains. It is known that as the alkyl side chain of the lubricant increases friction decreases.[2] However, the same reasoning is not valid when going from $[N_{1114}][C_4SO_3]$ to $[N_{1124}][C_1SO_3]$, where the friction coefficient increases, although the number of total carbon atoms passes from 11 to 12, respectively. For this, one can assume that an increase in the alkyl side chain of the cation induces a higher friction coefficient, although an increase of the alkyl side chain in the anion leads to a lower friction coefficient. In fact, it is known that the structural properties in the anion influence more significantly the tribological performance of the ionic liquid, when compared to the influence of the cation structure.

To understand the role of the alkyl side chains in the friction coefficient of these three ionic liquids, the orientational ordering parameter, $P_2(\theta)$, was again plotted in Figure 9. The graph concerning the ionic liquid $[N_{1114}][C_4SO_3]$ (Figure 9a) has already been discussed in Figure 8b, but it is also given here for a more direct comparison with the other two ionic liquids $[N_{1114}][C_1SO_3]$ and $[N_{1124}][C_4SO_3]$.

Figure 9 clearly establishes that the changes in the friction coefficient are also accompanied by changes in the orientation of the ionic liquid close to the surface. First, when the first layer closer to the surface is defined by parallel orientations, the friction coefficient is smaller (see Figure 9a). In opposite, when groups that are rather perpendicular to the surface occupy the first layer, the friction coefficient is higher (see Figure 9c). The difference between friction coefficients of parts b and c of Figure 9 may be explained by the fact that the ionic liquid $[N_{1124}][C_4SO_3]$ shows two different orientations in the same layer, which is not the case for $[N_{1114}][C_1SO_3]$, where the alkyl chains of cation and anion although oriented oppositely, occupy different layers at the surface. As discussed before, in the case of the ionic liquid $[N_{1114}][C_4SO_3]$ (Figure 9a), the cation and the anion alkyl chains are in phase with each other in the two layers close to the surface, which can promote the segregation of the nonpolar domains and decrease the friction coefficient of this last ionic liquid.

4. CONCLUSIONS

Here, we report a strategy to calculate the friction coefficient of ionic liquids interacting with surfaces. The calculation of the tangential and normal components of the pressure tensor in a two-slab geometry is the key solution to obtain accurate friction coefficients. We mimic the experimental conditions by performing nonequilibrium molecular dynamics simulations under a constant load and by moving one of the surfaces at constant velocity. The thermal and mechanical equilibrium are checked locally by plotting profiles of the temperature and pressure tensors along the direction where the heterogeneity takes place.

Once the methodology was developed, we investigated the dependence of the frictional forces on the load, shear velocity, surface topology, and nature of the ionic liquid. The simulated friction coefficients are in good agreement with the available experimental data, establishing our methodology as a quantitative method for the prediction of friction. The ionic liquid $[N_{1114}][C_4SO_3]$ was studied in contact with both a flat and a rough surface of iron. The molecular simulations predict a decrease in the friction when the ionic liquid interacts with the rough surface. This feature was interpreted in terms of the specific distribution of the charged groups of the ionic liquid and of the orientational order of the alkyl side chains close to the surface. A higher charge ordering in the interfacial layer seems to decrease the ability of the surface to slide and to promote higher friction coefficients. Besides, as the alkyl side chain in the anion increases, the orientation of both species tends to become parallel to the surface, which can promote the segregation of the alkyl side chains and facilitate sliding. The friction coefficient in this last case will be lower.

We have also explained the difference in the friction coefficients of different ionic liquids by exploring the orientations of the anions and cations close to the surface. The relationship between structure and rheological properties is far from being completely understood, and the methodology developed here represents a major step toward a better understanding of the origin of the lubricant properties of ionic liquids.

AUTHOR INFORMATION

Corresponding Author

*E-mail: Patrice.Malfreyt@univ-bpclermont.fr.

Notes

The authors declare no competing financial interest.

ACKNOWLEDGMENTS

The authors whish to acknowledge Dr. Stefan Eder from the Austrian Centre of Competence for Tribology (Wiener Neustadt, Austria) for the support with the nonequilibrium simulations. The work was granted access to the HPC resources of IDRIS under the allocation 2012-i2012092119 made by GENCI (Grand Equipement National de Calcul Intensif). This study was financed by the Marie Curie Initial Training Network MINILUBES (http://www.minilubes.net/) of the seventh Framework Program of the European Commission.

REFERENCES

(1) Bhushan, B.; Israelachvili, J. N.; Landman, U. *Nature* **1995**, *374*, 607.
(2) Minami, I. *Molecules* **2009**, *14*, 2286.
(3) Zhou, F.; Liang, Y. M.; Liu, W. M. *Chem. Soc. Rev.* **2009**, *38*, 2590.
(4) Palacio, M.; Bhushan, B. *Tribol. Lett.* **2010**, *40*, 247.
(5) Bermudez, M. D.; Jimenez, A. E.; Sanes, J.; Carrion, F. J. *Molecules* **2009**, *14*, 2888.
(6) Wasserscheid, P.; Welton, T. *Outlook*; Wiley-VCH Verlag GmbH & Co. KGaA: Berlin, 2003.
(7) Pensado, A.; Comuñas, M.; Fernández, J. *Tribol. Lett.* **2008**, *31*, 107.
(8) Kamimura, H.; Kubo, T.; Minami, I.; Mori, S. *Tribol. Intl.* **2007**, *40*, 620.
(9) Jimenez, A. E.; Bermudez, M. D.; Carrion, F. J.; Martinez-Nicolas, G. *Wear* **2006**, *261*, 347.
(10) Cai, M. R.; Liang, Y. M.; Yao, M. H.; Xia, Y. Q.; Zhou, F.; Liu, W. M. *ACS Appl. Mater. Interfaces* **2010**, *2*, 870.
(11) Cai, M. R.; Zhao, Z.; Liang, Y. M.; Zhou, F.; Liu, W. M. *Tribol. Lett.* **2010**, *40*, 215.
(12) Mahrova, M.; Vilas, M.; Domínguez, Á.; Gómez, E.; Calvar, N.; Tojo, E. *J. Chem. Eng. Data* **2012**, *57*, 241.
(13) Kamimura, H.; Chiba, T.; Kubo, T.; Nanao, H.; Minami, I.; Mori, S. *J. Jpn. Soc. Tribol.* **2006**, *51*, 826.
(14) Qu, J.; Truhan, J. J.; Dai, S.; Luo, H.; Blau, P. J. *Tribol. Lett.* **2006**, *22*, 207.
(15) Qu, J.; Blau, P. J.; Dai, S.; Luo, H. M.; Meyer, H. M.; Truhan, J. J. *Wear* **2009**, *267*, 1226.
(16) Stolte, S.; Steudte, S.; Igartua, A.; Stepnowski, P. *Curr. Org. Chem* **2011**, *15*, 1946.
(17) Stolte, S.; Steudte, S.; Areitioaurtena, O.; Pagano, F.; Thöming, J.; Stepnowski, P.; Igartua, A. *Chemosphere* **2012**, *89*, 1135.
(18) Baldelli, S. *Acc. Chem. Res.* **2008**, *41*, 421.
(19) Hayes, R.; Borisenko, N.; Tam, M. K.; Howlett, P. C.; Endres, F.; Atkin, R. *J. Phys. Chem. C* **2011**, *115*, 6855.
(20) Pensado, A. S.; Padua, A. A. H. *Angew. Chem., Int. Ed.* **2011**, *50*, 8683.
(21) Tazi, S.; Salanne, M.; Simon, C.; Turq, P.; Pounds, M.; Madden, P. A. *J. Phys. Chem. B* **2010**, *114*, 8453.
(22) Fedorov, M. V.; Lynden-Bell, R. M. *Phys. Chem. Chem. Phys.* **2012**, *14*, 2552.
(23) Mendonça, A. C. F.; Malfreyt, P.; Padua, A. A. H. *J. Chem. Theory Comput.* **2012**, *8*, 3348.
(24) Perkin, S.; Albrecht, T.; Klein, J. *Phys. Chem. Chem. Phys.* **2010**, *12*, 1243.
(25) Amontons, G. *Mémoires de l'Académie Royale A* **1699**, 257.
(26) Dowson, D. *History of Tribology*; Longman: London/New York, 1979.
(27) Israelachvili, J. N.; Berman, A. D. In *Handbook of Micro/Nanotribology*; Bhushan, B., Ed.; CRC Press: Boca Raton, 1999; p 371.
(28) Kapila, V.; Deymier, P. A.; Raghavan, S. *Model. Simul. Mater. Sci. Eng.* **2006**, *14*, 283.
(29) He, G.; Robbins, M. O. *Tribol. Lett.* **2001**, *10*, 7.
(30) He, G.; Robbins, M. O. *Phys. Rev. B: Condens. Matter* **2001**, *64*, 035413.
(31) Chandross, M.; Lorenz, C. D.; Stevens, M. J.; Grest, G. S. *Langmuir* **2008**, *24*, 1240.
(32) Chandross, M.; Grest, G. S.; Stevens, M. J. *Langmuir* **2002**, *18*, 8392.
(33) Salanne, M.; Madden, P. A. *Mol. Phys.* **2011**, *109*, 2299.
(34) Szlufarska, I.; Chandross, M.; Carpick, R. W. *J. Phys. D: Appl. Phys.* **2008**, 41.
(35) Eder, S.; Vernes, A.; Vorlaufer, G.; Betz, G. *J. Phys.: Condens. Matter* **2011**, 23.
(36) Vernes, A.; Eder, S.; Vorlaufer, G.; Betz, G. *Faraday Discuss.* **2012**, *156*, 173.
(37) Mazyar, O. A.; Jennings, G. K.; McCabe, C. *Langmuir* **2009**, *25*, 5103.
(38) Peters, G. H.; Tildesley, D. J. *Phys. Rev. E* **1996**, *54*, 5493.
(39) Irfachsyad, D.; Tildesley, D.; Malfreyt, P. *Phys. Chem. Chem. Phys.* **2002**, *4*, 3008.
(40) Goujon, F.; Malfreyt, P.; Tildesley, D. J. *Mol. Phys.* **2005**, *103*, 2675.
(41) Goujon, F.; Malfreyt, P.; Tildesley, D. J. *Macromolecules* **2009**, *42*, 4310.
(42) Cyrille Ibergay, P. M.; Tildesley, D. J. *J. Chem. Theory Comput.* **2009**, *5*, 15.
(43) Cyrille Ibergay, P. M.; Tildesley, D. J. *J. Phys. Chem. B* **2010**, *114*, 12.
(44) Jorgensen, W. L.; Maxwell, D. S.; TiradoRives, J. *J. Am. Chem. Soc.* **1996**, *118*, 11225.
(45) Kaminski, G.; Jorgensen, W. L. *J. Phys. Chem.* **1996**, *100*, 18010.
(46) Lopes, J. N. C.; Pádua, A. A. H. *J. Phys. Chem. B* **2004**, *108*, 16893.
(47) Lopes, J. N. C.; Pádua, A. A. H.; Shimizu, K. *J. Phys. Chem. B* **2008**, *112*, 5039.
(48) Finnis, M. W.; Sinclair, J. E. *Philos. Mag. A* **1984**, *50*, 45.
(49) Daw, M. S.; Baskes, M. I. *Phys. Rev. B: Condens. Matter* **1984**, *29*, 6443.
(50) Iori, F.; Corni, S. *J. Comput. Chem.* **2008**, *29*, 1656.
(51) Clarke, J. H. R.; Smith, W.; Woodcock, L. V. *J. Chem. Phys.* **1986**, *84*, 2290.
(52) Plimpton, S. *J. Comp. Phys* **1995**, *117*, 1.
(53) Braun, O. M. *Tribol. Lett.* **2010**, *39*, 283.
(54) Pensado, A.; Malfreyt, P.; Pádua, A. A. H. *J. Phys. Chem. B* **2009**, *113*, 14708.
(55) Kelkar, M. S.; Maginn, E. J. *J. Phys. Chem. B* **2007**, *111*, 4867.
(56) Hockney, R. W.; Eastwood, J. W. *Computer Simulation Using Particles*; Taylor and Francis: New York, 1989.
(57) Allen, M. P.; Tildesley, D. J. *Computer Simulation of Liquids*; Clarendon Press: Oxford, 1989.
(58) Irving, J. H.; Kirkwood, J. G. *J. Chem. Phys.* **1949**, *18*, 13.
(59) Walton, J.; Tildesley, D. J.; Rowlinson, J. S.; Henderson, J. R. *Mol. Phys.* **1983**, *48*, 1357.
(60) Ghoufi, A.; Goujon, F.; Lachet, V.; Malfreyt, P. *J. Chem. Phys.* **2008**, *128*, 16.
(61) Gao, J.; Luedtke, W. D.; Gourdon, D.; Ruths, M.; Israelachvili, J. N.; Landman, U. *J. Phys. Chem. B* **2004**, *108*, 3410.
(62) Derjaguin, B. *Z. Phys.* **1934**, *88*, 661.
(63) Gao, J. P.; Luedtke, W. D.; Gourdon, D.; Ruths, M.; Israelachvili, J. N.; Landman, U. *J. Phys. Chem. B* **2004**, *108*, 3410.
(64) Kronberger, M.; Pejaković, V.; Gabler, C.; Kalin, M. *Proc. Inst. Mech. Eng., Part J* **2012**, *226*, 933.
(65) Pejaković, V.; Kronberger, M.; Mahrova, M.; Vilas, M.; Tojo, E.; Kalin, M. *Proc. Inst. Mech. Eng., Part J* **2012**, *226*, 923.
(66) He, G.; Muser, M. H.; Robbins, M. O. *Science* **1999**, *284*, 1650.
(67) Lopes, J.; Padua, A. A. H. *J. Phys. Chem. B* **2006**, *110*, 3330.